Adsorption of Palladium Phthalocyanine on Graphite: STM and LEED Study

T. G. Gopakumar,* M. Lackinger, M. Hackert, F. Müller, and M. Hietschold*

Chemnitz University of Technology, Institute of Physics, Solid Surfaces Analysis Group, D-09107 Chemnitz, Germany

Received: December 8, 2003; In Final Form: March 31, 2004

Adsorption of planar palladium phthalocyanine (PdPc) molecules on the basal plane of graphite is studied using STM (sample at 50 K) and LEED under UHV condition. The monolayer was grown in-situ by organic molecular beam epitaxy (OMBE) on the substrate at room temperature. PdPc molecules diffuse freely on the graphite substrate and form highly ordered, almost defect-free monolayers with a quadratic lattice. One lattice vector of the molecular adlattice is rotated by ±10° with respect to one of the graphite lattice vectors. On the basis of the high-resolution STM images, a model of the adlayer primitive unit cell is proposed, which reveals the adsorption geometry of PdPc molecules on graphite. For a better understanding of the submolecular contrast, the software package Gaussian 98 was used to calculate the electronic structure of isolated PdPc molecules. The STM contrasts at positive sample bias can be assigned to the wave function of the LUMO.

Introduction

Molecular nanostructures formed by the self-assembly of organic molecules on crystalline substrates have received remarkable attention during the last few decades. The knowledge of molecule−molecule and molecule−substrate interactions (typically of noncovalent type) is important to fabricate these nanostructures from different molecular species. It provides the opportunity to look at a more localized physical process during the self-assembly. A variety of molecules exist among which phthalocyanines are well known for the formation of ordered structures on different crystalline substrates.[1,2] They belong to an interesting class of organic dye molecules, which have a stable extended π-electron system and a structural analogy with biomolecules such as chlorophyll, vitamine B_{12}, hemoglobin, and so forth. The tunability of their electronic and structural properties by the selective addition of a metal atom to the central cavity makes these molecules ideal for studies in fundamental science and technological applications such as optoelectronic devices,[8−10] sensors,[11] solar cells,[12,13] etc.

Many STM experiments have been performed with different metal phthalocyanine (MePc), especially planar molecules, like CuPc,[1,2,14] NiPc,[15] FePc,[15] CoPc,[14,16] and so forth, on different substrates. In fact, CuPc is one of the first molecules ever imaged by STM.[13] Many groups investigated the crystallographic and electronic structure of adsorbed CuPc molecules on different substrates. For example, Lippel et al. studied CuPc on Cu(100)[12] and Kanai et al. investigated the adsorption of CuPc on Si(100) and (111) surfaces.[17] Results on nonplanar phthalocyanines such as SnPc[18] and PbPc[19] have been reported. These systematic studies of molecular adsorbates by carefully changing the electronic and structural properties of the molecules open a new way to understand more about the adsorption properties of these molecules.

Different reports on metal phthalocyanines show that, depending on the central metal atom, there arise significant differences in the STM contrast especially at the center of the molecule. Hipps et al. reported a depression at the center of single molecules in NiPc and CuPc and a protrusion in FePc and CoPc at the center of the STM images of single molecules.[15,16] This arises because the completely filled or unfilled d_{z^2} orbital of the metal atom is energetically far from the Fermi level and does not contribute to the HOMO and LUMO of the molecule, respectively. These frontier orbitals are mainly comprised of π-electrons of carbon and nitrogen atoms. It would be interesting to understand more about the d-orbital contribution near HOMO and LUMO to the STM contrast of Pc molecules, which contain metal atoms of higher atomic number like Pd, Pt, and so forth. To the best of our knowledge, the real-space studies of these MePc adlayers on crystalline substrates have not been reported so far. These studies may reveal the changes in structural and electronic properties of such metal phthalocyanines and the influence of the rather large metal atoms in the adlayer formation. In this work, we have investigated the adsorption of palladium phthalocyanine (PdPc) on graphite using STM and LEED. The molecular orbitals of PdPc are simulated by restricted Hartree−Fock method (RHF) and density functional theory (DFT) and compared with the STM results.

Experimental Section

PdPc was purchased with a purity of 99% from Aldrich. The monolayers are prepared by organic molecular beam epitaxy (OMBE) with the sample held at room temperature and with a background pressure around 10^{-10} mbar. The evaporation rate is controlled by a quartz microbalance, which was calibrated by subsequent in-situ STM and LEED measurements. The deposition rate measured by quartz crystal microbalance is approximately 0.25 nm/min for 3 min from previously degassed molecules. Graphite is freshly cleaved and annealed at 550 °C for 12 h prior to the deposition. Electrochemically etched tungsten tips were used for the investigation, and all tips are cleaned by subsequent Ar^+-ion sputtering and several heating cycles up to 700 °C. Experiments are carried out at 50 K sample temperature in a VT-STM from Omicron equipped with sample cooling by a liquid helium flow cryostat. The LEED experiments

* To whom correspondence should be addressed. Fax: +49 371 531 3181; e-mail: thiruvacheril.gopakumar@physik.tu-chemnitz.de (T. G. Gopakumar). Fax: +49 371 531 3181; e-mail: hietschold@physik.tu-chemnitz.de (M. Hietschold).

10.1021/jp037751i CCC: $27.50 © 2004 American Chemical Society
Published on Web 05/18/2004

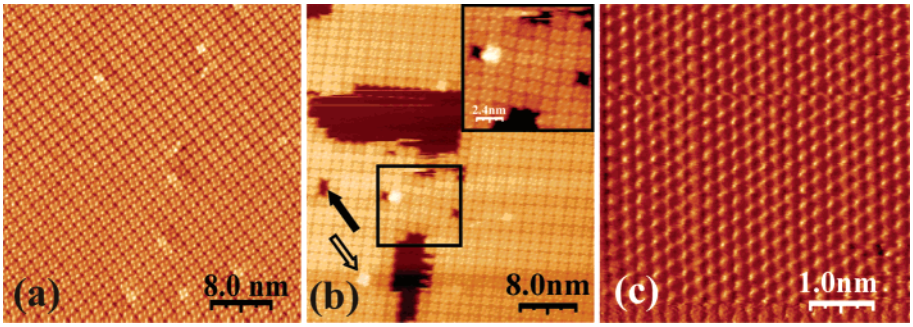

Figure 1. (a) and (b) are the STM constant current topographies of PdPc monolayer taken from different areas on the sample with a positive sample bias (+1.2 V) and a tunneling current of 75 pA. (a) A nearly defect-free adlayer of PdPc on graphite. (b) Different kind of defects: the solid arrow highlights missing molecules and the hollow arrow shows a single molecule adsorbed on top of the monolayer; the inset shows the magnification of the dislocation defect. (c) Constant current image of graphite (+68 mV and 1.04 nA) taken within the uncovered (dark) region near the center of Figure 1b.

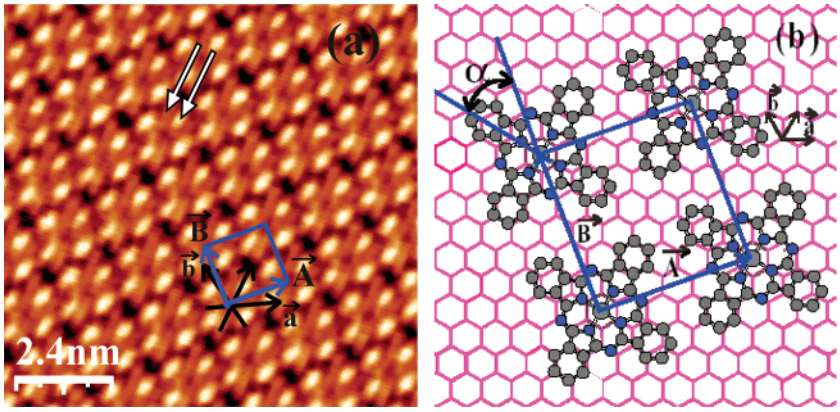

Figure 2. (a) STM constant current image of PdPc (1.2 V, 75 pA); the square represents the unit cell of the molecular adlayer with the vectors $\vec{A}$ and $\vec{B}$. (b) Schematic representation of a unit cell of PdPc monolayer on a graphite sheet (deduced from the images 1 and 2a, hydrogen atoms are not shown). Vectors of the adlayer ($\vec{A}$,$\vec{B}$) and graphite ($\vec{a}$, $\vec{b}$) are marked and α is the azimuthal angle.

are carried out in the same UHV system with a SpectraLEED from Omicron.

Results and Discussions

PdPc molecules form ordered and defect-free monolayers as shown in Figure 1a. However, the image is a part of the adlayer, which extends up to 500 × 500 nm^2. This indicates a sufficient mobility of the adsorbate during the film growth. The symmetry of a single molecule is in accordance with molecules adsorbed with their plane parallel to the substrate. Obviously, this geometry optimizes the interaction of the extended π-electron cloud with the graphite substrate. Some regions show defects and dislocation, which are shown in Figure 1b. The inset of Figure 1b shows an example for a dislocation due to two laterally shifted domains. The solid arrow and hollow arrow in the figure depict point defects due to missing molecules or an additional molecule on top of the adlayer, respectively. Figure 1c shows the graphite lattice taken at a pristine substrate region in the center of Figure 1b. Atomic resolution of the graphite substrate was possible for appropriate imaging parameters, thereby revealing the relative orientation to the adsorbate lattice.

Figure 2a shows a high-resolution STM picture of a densely packed PdPc monolayer. We can see a nearly symmetric crosslike structure with a depression at the center, which can be attributed to a single molecule. The square indicates the unit cell with $\vec{A}$ and $\vec{B}$ as the base vectors of the adsorbate lattice. Within the experimental error, the primitive unit cell is quadratic with lattice vectors $\vec{A} \approx \vec{B} = 1.4 \pm 0.1$ nm and an angle $\theta = 90 \pm 2°$ between them. In contrast, Freund et al. found a hexagonal symmetry for metal-free Pc molecules on graphite.[20]

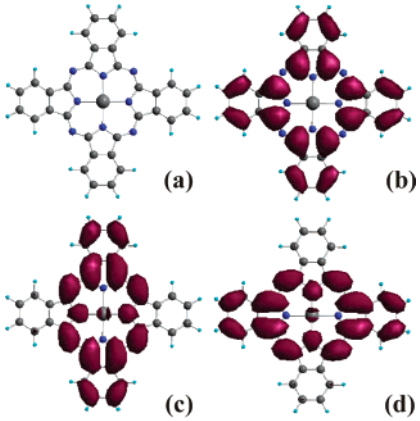

Figure 3. Molecular orbital calculations for isolated PdPc molecules using Gaussian 98 with density functional theory (B3LYP/3-21G). Molecular structure (a), HOMO (b), and degenerate LUMOs (c) and (d).

The submolecular resolution shows the relative orientation of molecules within the adlattice, and hence, determines the azimuthal angle α between $\vec{B}$ and the molecular axis to 35 ± 2°. In contrast to the expected fourfold symmetry of the single molecules, Figure 2a shows a stripelike structure passing through the molecule. Two of these adjacent stripes are marked with arrows and are separated by 2.5 ± 0.1 Å, which is similar to the graphite lattice constant. The contrast of these stripes is more pronounced when the tunneling current is higher. This is reasonable because when the tip−sample distance is less, then the involvement of substrate orbitals in the tunneling process is possible, and they become visible. The same kind of

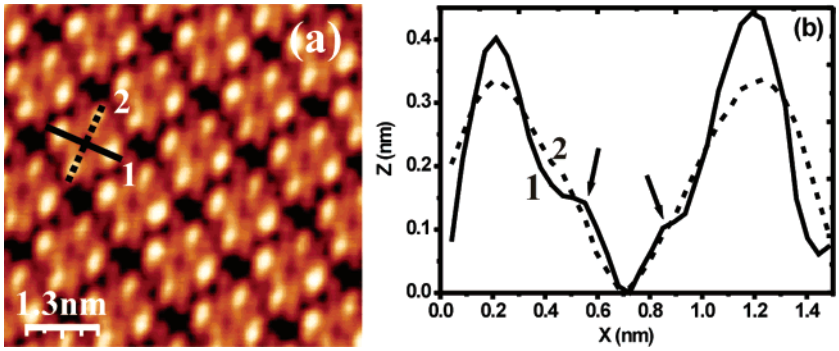

Figure 4. (a) High-resolution STM constant current topography of PdPc (1.2 V, 75 pA). (b) Comparative line profiles through the perpendicular lobes of a molecule (marked with a solid and dotted line in figure a).

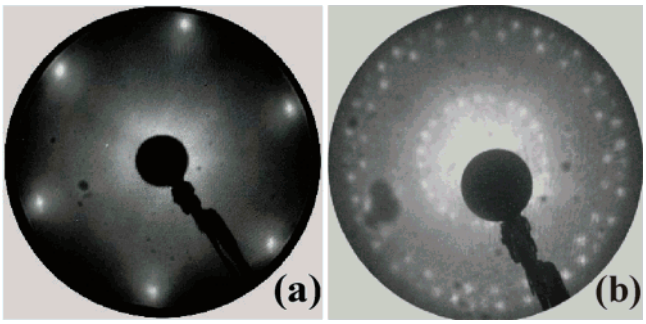

Figure 5. (a) LEED pattern of annealed graphite taken at 63 eV and (b) PdPc on graphite at 15 eV.

observation was made in the case of naphthalocyanine on graphite.[21] $\vec{a}$, $\vec{b}$ in the figure are the assumed graphite lattice directions from the additional contrast. One of the molecular lattice vectors $\vec{B}$ shows a rotation of 10 ± 1° from $\vec{b}$. This is consistent with the rotational angle measured from the image of graphite (Figure 1c) taken at the uncovered substrate region near the center of Figure 1b. These observations show that the molecules are not aligned with the graphite lattice but are rotated by 10 ± 1°, as a consequence of adsorbate−substrate interaction. Moreover, the contrast line of graphite lattices is never found passing through the center of the molecules. This may be due to the relatively large size of the palladium atom. However, the comparable size of the atomic radius of Pd atom (1.35 Å) with the graphite lattice spacing opens up the possibilities for the Pd atoms to sit above the center of benzene rings of the graphite sheet. In addition, the contrast corresponding to two lobes of the PdPc molecule are aligned along these stripes. This suggests a registry of molecules with one of the graphite lattice directions. To prove the observations made from the figure, we elucidated a model for the quadratic unit cell of the molecular superlattice on the graphite sheet, which is shown in Figure

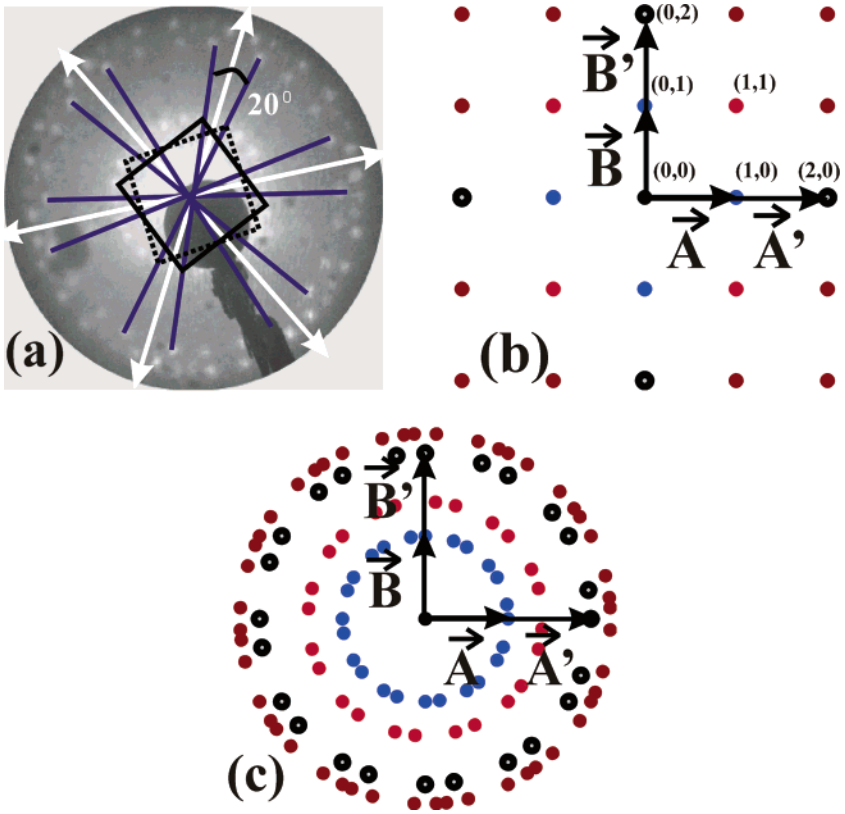

Figure 6. (a) Experimental LEED patterns, double-headed arrows represent the direction of graphite lattice vectors visible at higher energies. Squares depict two unit cells from different rotational domains of the molecular adlayer. (b) Shows the geometric LEED simulation for a single quadratic lattice, first and second orders of diffraction are marked using $\vec{A}$,$\vec{B}$ (reciprocal unit vectors) and $\vec{A}'$, $\vec{B}'$, respectively. (c) Simulation of six rotational domains of quadratic lattice.

2b. The adsorbate lattice vectors ($\vec{A}$,$\vec{B}$) and the graphite lattice vectors ($\vec{a}$, $\vec{b}$) are marked. The azimuthal orientation or the rotation of molecule with respect to the adlattice is represented by α. The model shows clearly the adsorption geometry of single molecules in the adlayer and also the relative orientation of the molecular superlattice to the graphite lattice. All observations made in the real-space images are consistent with the model.

For a better understanding of the contrast of high-resolution images taken at different tunneling voltages, molecular orbitals are calculated using the restricted Hartree−Fock method and density functional theory implemented in Gaussian 98.[22] Figure 3 shows the Gaussian output for energetically optimized geometry of molecule (a), HOMO (b), and degenerated LUMOs (c) and (d). The HOMO has a highly symmetric flowerlike structure with a big hole at the center. Moreover, the LUMO was doubly degenerated with a twofold spatial symmetry. These degenerate orbitals are reported also for several other metal phthalocyanines.[23] Both calculation methods show similar results for the spatial symmetry of the HOMO and LUMO wave functions.

Figure 4a shows the STM image taken at a positive sample bias and Figure 4b shows the line profiles from a single molecule as marked in the image (each line runs along one of the orthogonal axes of PdPc). Both line profiles show in principle similar characteristics; however, curve 1 has two shoulders near the center as marked by arrows. This arises because of the extra contrast from the graphite substrate, which has been discussed in the previous section. Each curve contains a central minimal point corresponding to the binding site of the metal atom and the peaks representing the benzene rings of the molecule. This is a clear indication that the unfilled molecular orbitals, which have contributions from the metal d-orbitals, are far away from the Fermi edge in accordance with our calculations. The LUMO consists mainly of π-orbitals, which are delocalized over the benzene rings. The single molecule STM image shows four lobes. In contrast, the twofold symmetry of the LUMOs suggest that both LUMOs are involved in the tunneling process. So, the image corresponding to a single molecule is likely to be a superposition of these two degenerated orbitals. The peaks in curve 2 are lower compared to that in curve 1. The benzene rings, which correspond to these peaks, are located above the ring center of the graphite lattice. The overlap of the π-electrons of these benzene rings with the graphite, as seen in the model in Figure 2b, may be the reason that they are less pronounced in the STM.

Figure 5a shows the typical LEED pattern taken at electron energy of 63 eV for graphite and b is the corresponding pattern for PdPc molecules on graphite at 15 eV. The clear and separate spots in the LEED pattern of PdPc molecules on graphite indicate a high degree of ordering. Moreover, this adlayer is stable to the high-energy electron beam and also to high beam currents during LEED measurements for more than 10 min. However, the spots seem to be vanishing when the sample is heated above 70 °C and they did not reappear after cooling. In contrast to STM imaging, LEED provides an averaged structural information over a large area of the sample. Different phthalocyanines were extensively studied using LEED. Buchholz et al. observed quadratic lattices for phthalocyanine on different copper surfaces;[26] Cox et al. observed the hexagonal lattice for CuPc molecules on InAs and InSb surfaces[27] and England et al. observed the same kind of diffraction pattern for InPcCl and CuPc on MoS_2 and SnS_2.[28]

In Figure 6a, the double-headed arrows represent the orientation of graphite and the black lines represent the respective orientation of molecular superlattice with graphite. Squares represent two unit cells corresponding to quadratic lattices, which arise from two different rotational domains of the molecular adlattice. These unit cells are rotated by $\pm 10°$ from the respective graphite lattice vector. This shows that there exist two different rotational domains for each graphite lattice direction. So, the observed diffraction pattern can be explained by the superposition of six (3×2) rotational domains of the quadratic lattice. Figure 6b shows a single quadratic lattice and 6c shows six rotational domains of quadratic lattice. $\vec{A}$,$\vec{B}$ (reciprocal unit vectors) and $\vec{A}'$, $\vec{B}'$ represent first and second order of diffraction, respectively. The ratios of $\vec{A}$ to $\vec{A}'$ and $\vec{B}$ to $\vec{B}'$ in the simulation and the ratio of radii of first to second ring in the experiment is 0.5 and are consistent with the assumed order of the LEED spots. To determine the unknown lattice vectors of the molecular adsorbates, the inverse of square root of energy versus distance of the first-order spot (from the center) of molecular adsorbates and graphite are plotted as discussed in the previous paper.[29] From the slope of each curve, the molecular lattice vectors $\vec{A} \approx \vec{B} = (1.30 \pm 0.05)$ nm are calculated using $A_{mol} = (\text{slope}_{gra}/\text{slope}_{mol} * a_{gra})$. These values show a small discrepancy with the STM results. This may be explained by the relative error in the STM measurement arising in general because of the drifts during the measurements and piezo calibration.

Conclusion

The adsorption of PdPc molecules on graphite have been investigated using variable temperature STM and LEED. For the monolayer covered areas, a quadratic lattice of molecular adsorbates was observed. STM and LEED show that the quadratic adlattice of molecules are rotated by $\pm 10°$ with respect to graphite lattice. Because of the substrate symmetry, this leads to the existence of six different rotational domains. Moreover, we compared the STM observations using a first-principle calculation of molecular orbitals of PdPc. The STM images taken at positive sample bias voltage are consistent with the observed degenerate LUMOs in the calculation.

Acknowledgment. T.G.G thanks the Deutsche Forschungsgemeinschaft for the financial support within the Graduate College Accumulation of Single Molecules to Nanostructures.

Supporting Information Available: Image of a constant current topograph of PdPc on graphite. This material is available free of charge via the Internet at http://pubs.acs.org.

References and Notes

(1) Gimzewski, J. K.; Stoll, E.; Schlittler, R. R. *Surf. Sci.* **1987**, *181*, 267−277.

(2) Yoshimoto, S.; Tada, A.; Suto, K.; Itaya, K. *J. Phys. Chem. B* **2003**, *107*, 5836−5843. (b) Suto, K.; Yashimoto, S.; Itaya, K. *J. Am. Chem. Soc.* **2003**, *125*, 14976−14977.

(3) Fan, F.; Faulkner, L. R. *J. Chem. Phys.* **1978**, *69*, 3334−40.

(4) Fan, F.; Faulkner, L. R. *J. Chem. Phys.* **1978**, *69*, 3341−49.

(5) Minami, N.; Asai, M. *Jpn. J. Appl. Phys.* **1991**, *30*, L643−L646.

(6) Yong, Q.; Yudi, G.; Peng, W.; Liduo, W. *Appl. Phys. Lett.* **2002**, *80*, 2628−2630.

(7) Yamashita, A.; Matsumoto, S.; Sakata, S.; Hayashi, T.; Kanbara, H. *J. Phys. Chem. B* **1998**, *102*, 5165−5167.

(8) Wang, S.; Liu, Y.; Huang, X.; Yu, G.; Zhu, D. *J. Phys. Chem. B* **2003**, *107*, 12639−12642.

(9) Hone, D. C.; Walker, P. I.; Evans-Gowing, R.; FitzGerald, S.; Beeby, A.; Chambrier, I.; Cook, M. J.; Russell, D. A. *Langmuir* **2002**, *18*, 2985−2987.

(10) Xiao, K.; Liu, Y.; Huang, X.; Xu, Y.; Yu, G.; Zhu, D. *J. Phys. Chem. B* **2003**, *107*, 9226−9230.

(11) Collins, R. A.; Mohammed, K. A. *J. Phys. D* **1988**, *21*, 154−161.

(12) Ghosh, A. K.; Morel, D. L.; Feng, T.; Shaw, R. F.; Rowe, C. A. *J. Appl. Phys.* **1974**, *45*, 230−236.
(13) Amao, Y.; Komori, T. *Langmuir* **2003**, *19*, 8872−8875.
(14) Lippel, P. H.; Wilson, R. J.; Miller, M. D.; Wöll, Ch.; Chiang, S. *Phys. Rev. Lett.* **1989**, *62*, 171−174.
(15) Xing, Lu.; Hipps, K. W. *J. Phys. Chem. B* **1997**, *101*, 5391−5396.
(16) Hipps, K. W.; Xing, Lu.; Wang, S. D.; Mazur, U. *J. Phys. Chem. B* **1996**, *100*, 11207−11210.
(17) Kanai, M.; Kawai, T.; Motai, K.; Wang, X. D.; Hashizume, T.; Sakura, T. *Surf. Sci.* **1995**, *329*, L619−L623.
(18) Lackinger, M.; Hietschold, M. *Surf. Sci.* **2002**, *520*, L619−L624.
(19) Ottaviano, L.; Lozzi, L.; Santucci, S.; Di Nardo, S.; Passacantando, M. *Surf. Sci.* **1997**, *392*, 52−61.
(20) Freund, J.; Probst, O.; Grafström, S.; Dey, S.; Kowalski, J.; Nehmann, R.; Wörtge, M.; Putlitz, zu, G. *J. Vac. Sci. Technol. B* **1994**, *12*, 1914−1917.
(21) Lackinger, M.; Müller, T.; Gopakumar, T. G.; Müller, F.; Hietschold, M.; Flynn, G. W. *J. Phys. Chem. B* **2004**, *108*, 2279−2284.
(22) Frisch, M. J. et al. *Gaussian 98*, Revision A.9; Gaussian, Inc.: Pittsburgh, PA, 1998.
(23) Liao, M.; Scheiner, S. *J. Chem. Phys.* **2001**, *114*, 9780−9791.
(24) Hishino, A.; Isodo, S.; Kurata, H.; Kobayashi, T. *J. Appl. Phys.* **1994**, *76*, 4113−4120.
(25) Reiter, M. M.; Jamitzky, F.; Trixler, F.; Heckl, W. M. *Phys. Status Solidi* **2001**, *187*, 171−176.
(26) Buchholz, J. C.; Somorjai, G. A. *J. Chem. Phys.* **1977**, *66*, 573−580.
(27) Cox, J. J.; Jones, T. S. *Surf. Sci.* **2000**, *457*, 311−318.
(28) England, C. D.; Collins, G. E.; Shuerlein, T. J.; Armstrong, N. R. *Langmuir* **1994**, *10*, 2748−2756.
(29) Lackinger, M.; Griessl, S.; Heckl, W. M.; Hietschold, M. *J. Phys. Chem. B* **2002**, *106*, 4482−4485.